

PAPER

Feedback control of stored energy and rotation with variable beam energy and perveance on DIII-D

To cite this article: M.D. Boyer *et al* 2019 *Nucl. Fusion* **59** 076004

View the [article online](#) for updates and enhancements.

Feedback control of stored energy and rotation with variable beam energy and perveance on DIII-D

M.D. Boyer¹, K.G. Erickson¹, B.A. Grierson¹, D.C. Pace²,
J.T. Scoville², J. Rauch², B.J. Crowley², J.R. Ferron², S.R. Haskey¹,
D.A. Humphreys², R. Johnson², R. Nazikian¹ and C. Pawley²

¹ Princeton Plasma Physics Laboratory, Princeton, NJ 08543, United States of America

² General Atomics, San Diego, CA 92121, United States of America

E-mail: mboyer@pppl.gov

Received 7 January 2019, revised 14 March 2019

Accepted for publication 10 April 2019

Published 22 May 2019



CrossMark

Abstract

Design and testing of a new method for real-time control on DIII-D using the new voltage and perveance variation capability of DIII-D's neutral beam injection system is presented. The approach enables control of power, torque, stored energy, and rotation without requiring pulse-width modulation of the beams. Such modulations are perturbative to experiments, can cause beam reliability problems, and could potentially damage or fatigue accelerator grids, especially looking forward to active control of long-pulse devices and reactors. The control algorithm accounts for beam line loss mechanisms and includes approaches that address the complexity of having three manipulated variables for each of the eight beams and compensate for the rate and magnitude limits affecting the voltage and perveance actuators. Results are presented that demonstrate the performance of the approach in the first feedback control experiments to use the expanded controllability of the DIII-D beams.

Keywords: neutral beams, plasma control, rotation control

(Some figures may appear in colour only in the online journal)

1. Introduction

Neutral beam injection provides a source of power, particles, current, and torque to tokamak plasmas and is one of the primary actuators used for real-time plasma control on many devices. A typical approach to controlling the injected power used by DIII-D, NSTX-U, and others, is to use short injection pulses and pulse width modulation to achieve a time-varying average power at fixed beam energy. Alternative means of in-shot variation of beam power have been achieved on MAST [1] (altering source current) and TEXTOR [2] (altering beam line aperture). In support of DIII-D steady state scenario study goals, upgrade plans aim at increasing injected power by increasing beam energy [3, 4], however, the existence of beam ion driven instabilities can cause reduced confinement or enhanced fast ion losses [5, 6], motivating the development of new methods of tailoring the fast ion distribution. While changes in beam

geometry can significantly impact the stability of fast ion modes (e.g. increased tangency radius beam injection was shown to eliminate certain modes on NTSX-U [7]), real-time variation of the injection energy and power could provide the flexibility needed to actively optimize the heating, current drive, torque, and confinement in the scenarios of interest.

This novel capability has recently been added to the DIII-D neutral beam injection system, enabling simultaneous in-shot variation of beam energy and current for the first time [8, 9]. This new capability is now being explored as a tool for integrated plasma control, aiming toward optimization of the fast ion distribution for control of equilibrium profiles and Alfvén eigenmode activity [10, 11]. For example, beams can inject at lower energy during the current ramp and at higher energy later in the discharge. The approach allows continuous variation of power and torque, in contrast to the typically used, but perturbative, pulse-width-modulation approach to power

and torque control. This can be especially important in experiments studying low-torque scenarios. Real-time variation of voltage and perveance improves controllability while at the same time avoiding the need for beam modulations or operation far from optimal beam perveance, which can damage or fatigue accelerator components and high voltage power supplies. Enabling flexible control while avoiding fatigue on critical components could be especially important for long-pulse experiments and future reactors.

The existing pulse width modulation approach to modifying the injected beam power during shots has been actively used on DIII-D for years to enable both feedforward control, e.g. power and torque ramps, and feedback control, e.g. control of plasma beta and/or rotation [12]. Recently, beam modulation has been used, along with other actuators, including the gyrotrons, gas fueling, and loop voltage, to control the current profile on DIII-D [13–16]. Modulation of the beam power has also been recently used to modify the drive for Alfvén eigenmode activity based on feedback from ECE measurements [17]. Each of these applications stands to benefit from the additional flexibility of having in-shot variation of beam voltage and perveance as a less perturbative approach to modifying heating, current drive, torque, and instability drive.

The outputs of the DIII-D plasma control system (PCS) [18, 19] have been extended to include signals that can be used to alter the beam voltage and current [8, 9]. In this work, the new actuation approach is used as part of a feedback algorithm for the first time by expanding upon the algorithm for stored energy and rotation control presented in [12]. Control approaches are included in the algorithm to address the nonlinear behavior of the beams, the increased number of available actuators, and constraints that must be respected to ensure beam reliability. These advances are expected to contribute to the development of more sophisticated applications of the expanded controllability enabled by the new actuation methods for feedback control, including active profile and fast ion phase space control. The paper is organized as follows: section 2 provides an overview of the control approach designed and tested in this work. Section 3 describes results of experimental testing on the DIII-D tokamak. A discussion of results and future plans is provided in section 4, while details of the control-oriented modeling and algorithm design are provided in appendices A and B, respectively.

2. Control design overview

The goal of the control design is to provide control of either the total injected beam power, the plasma stored energy, or β_N , while simultaneously controlling torque or the plasma toroidal rotation velocity at a single radial location, expanding the often used capability developed in [12] to take advantage of the new variable beam voltage and perveance capabilities.

2.1. Real-time measurements

The stored energy and β_N are estimated in real-time by rtEFIT [20], the real-time equilibrium reconstruction code.

The rotation velocity is calculated in real-time from impurity charge-exchange emission from heating beams. In this work, a single channel from the CER system is selected at any given time for use in feedback control calculations. Since each channel has an associated heating beam line that it views, the choice of channel forces one of the heating beams to be on, or at least modulated with a large enough duty cycle to achieve high enough signal to noise ratio for fitting. The duty cycle effectively determines the rate at which new rotation measurements become available in real-time, with the highest rate at 100% duty cycle.

2.2. Real-time actuators

The DIII-D neutral beam system has eight beams: six that inject in the same direction as the plasma current (these beams are called 30L, 30R, 150L, 150R, 330L, and 330R) and two that inject in the counter-current direction (210L and 210R). In total, there are 24 potential beam variables manipulated from the PCS (voltage, perveance, and duty cycle for each of the eight beams). At this time, all beams except 30R allow variable beam voltage and perveance, resulting in 22 manipulated variables and two outputs to be controlled. While the problem as posed is under constrained, future efforts to control Alfvén eigenmode activity and the deposition profiles of heating, torque, and current drive will expand the number of outputs to be controlled through manipulation of these beam variables. Furthermore, each actuator has magnitude constraints that depend on both technical considerations and the requirements for a particular experiment. For example, the 30L beam may be constrained to operate at 81 kV and to modulate with a fixed pattern based on the requirement to obtain motional Stark effect measurements to reconstruct the current profile.

Due to power dissipation limits on the tetrode in the modulator/regulators, the voltage can be varied in-shot within a range of ± 10 kV around the nominal that is set before the shot. To ensure that remaining ions leaving the neutralization stage are bent into beam dumps, the bending magnet current must precisely change in response to changes in beam voltage. Due to power supply limitations, the bending magnet current changes slowly compared to the potential rate of change of the voltage, and an interlock is put in place to shut down the beam if the voltage is changed too quickly. To avoid tripping this interlock, it is necessary to observe voltage rate limits of $20\text{--}40$ kV s^{-1} (each beam has different power supplies).

For a given source operating point (beam voltage, beam current, arc power), there is an optimal value of perveance to minimize beam divergence. This optimal value depends on the geometry of the acceleration grids and the extracted ion species mix. Moving too far from this optimal can send power to unintended areas within the beam line or result in arcing. This can result in reduced beam reliability (e.g. temporary beam blocking). If too many blocks occur, the beam interlocks disable the beam for the remainder of the shot. To maintain beam reliability, it is necessary for the perveance to remain within a range of typically $\pm 10\%$ of the empirically identified optimal perveance $\Pi_{\text{opt}}(V)$.

The typically used beam modulation approach introduces strong nonlinearities in the response of the beams, first as a result of turning the beams on and off, but also as a result of technical restrictions on the timing of each modulation. If a beam is turned off, it must remain off for 10 ms. For a fixed modulation period (usually taken to be on the order of the beam slowing down time) this limit results in dead zones in the response of the beams when requesting duty cycles close to zero or one. For experiments requiring precise timing and control over the beam characteristics, these nonlinearities represent a challenge. Since many plasma diagnostics depend on light emitted as a result of beam injection, beam modulations can temporarily ‘blind’ a diagnostic. For example, beam modulations used by a toroidal rotation velocity feedback control algorithm to modify beam torque may reduce the frequency at which reliable velocity measurements are available. Finally, experiments relying on precise conditions, for example studies of plasma at zero beam torque, can be severely perturbed or become difficult to analyze as a result of beam modulations.

Modifying the voltage and perveance of the beams provides a means of smoothly varying the beams that are actively injecting. However, since the allowable ranges of voltage and perveance changes are limited for the technical reasons described previously, beam modulations can still be required for large changes in power, torque, or current drive. Problems associated with beam modulation cannot be avoided entirely and the beam control configuration must be carefully considered when designing experiments. For example, it may be desirable to allow beam modulations during specific parts of a discharge (when large changes in plasma parameters are required) or to temporarily enable them for short transients (to quickly respond to large changes in required beam power) while avoiding modulations throughout the remainder of the shot.

2.3. Algorithm description

Based on the previous considerations, it is important that the control scheme can handle the multivariable nature of the problem, along with the constraints on the manipulated variables. It is also desirable for the algorithm to incorporate as much of the known beam system dynamic behavior into the decision making process as possible, and to avoid high sensitivity to noise in the measured values used for feedback. The real-time control system CPU that was available for implementation of the algorithm has a cycle time of 50 μ s, and, based on the other functions running on the CPU, the proposed control algorithm must execute in less than 20 μ s.

The control design approach used in this work is a model-based multi-input-multi-output (MIMO) scheme that builds off of the design proposed for controlling non-inductively sustained scenarios in NSTX-U [21]. It embeds the nonlinear dependence of power and torque on the actuators, as well as simplified models for the response of the stored energy and rotation to power and torque changes in the control law. The approach also mitigates the effects of actuator dynamics and

saturation on the performance of the closed-loop system through constrained real-time optimization. This enables the algorithm to make the most of the available actuators while actively avoiding exceeding voltage and perveance values that would impact beam reliability. Because of the slow response of the beam voltage to requested changes, a two-time scale approach is used in which the voltage changes respond to low frequency tracking errors, while the faster actuators, perveance and duty cycle changes, are changed to compensate at faster time scales. While not as sophisticated and powerful as a nonlinear constrained model predictive control algorithm, the approach used in this work requires significantly less calculation time. More sophisticated approaches will be considered in the future, but will require hardware upgrades (additional real-time CPUs) to be implemented in the DIII-D PCS.

The approach, depicted in figure 1, includes the following parts:

- (i) A dynamic observer to estimate the energy and rotation velocity from noisy measurements. The observer, which was not a part of the modulation-based algorithm presented in [12], provides smooth estimates of the controlled quantities as well as estimates of low frequency power and torque disturbances that can be rejected by the available actuators.
- (ii) An optimization of adjustments to the reference actuator trajectories (voltage, perveance, and duty cycle) to minimize the steady-state error between achieved outputs and the operator-provided target values. The disturbances estimated by the observer are included here, ensuring that (in the absence of actuator limits and assuming constant targets) the system converges to zero steady-state tracking error. The limits of the actuators are taken into consideration as well, ensuring the tracking error is minimized within the reliable range of the beam parameters. The disturbance estimation and constrained optimization approach avoids the problems with integrator wind-up found in PID algorithms, like the one used in [12].
- (iii) A feedback control law to adjust the power and torque requests calculated in (ii) to improve response time of the system and respond to high frequency disturbances.
- (iv) An optimization of the perveance and duty cycle to optimally track the feedback augmented power and torque requests calculated in (iii). In this optimization, the voltage is considered fixed at its presently estimated value. This enables the faster perveance and duty cycle actuators to compensate for the slowly changing voltage as it moves toward the steady-state value calculated in (ii). This approach enables the slow voltage changes to be used for low-frequency control, and the faster perveance and duty cycle changes to be used for higher frequency response improvement.

Details of the dynamic models used for control development are provided in appendix A, while the detailed design of the control algorithm is described in appendix B.

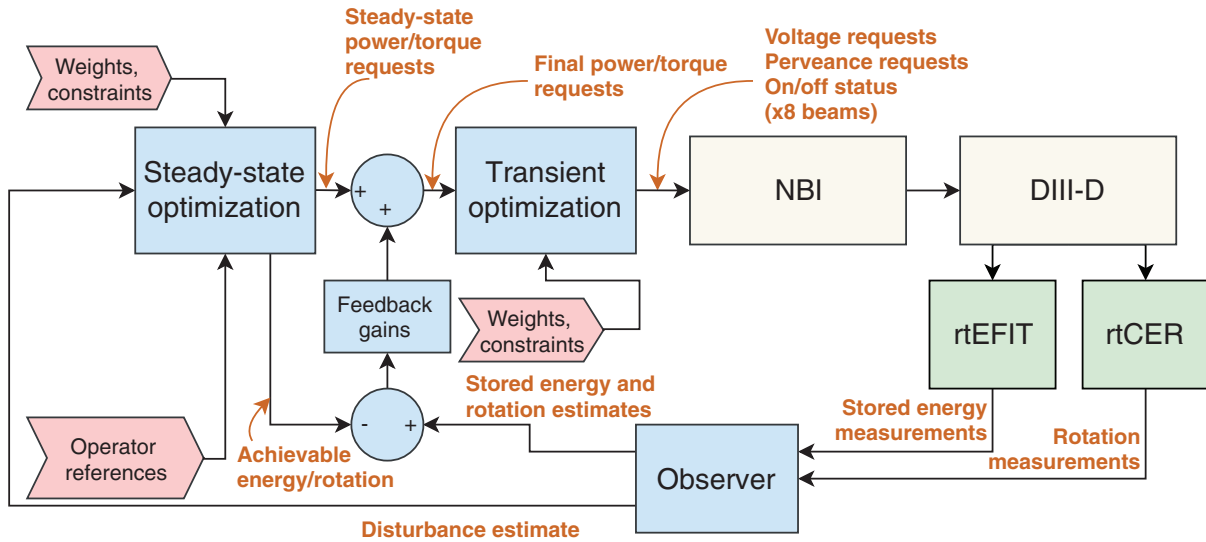


Figure 1. Schematic of multi-input multi-output control algorithm including observer, steady-state optimization, feedback, and transient optimization.

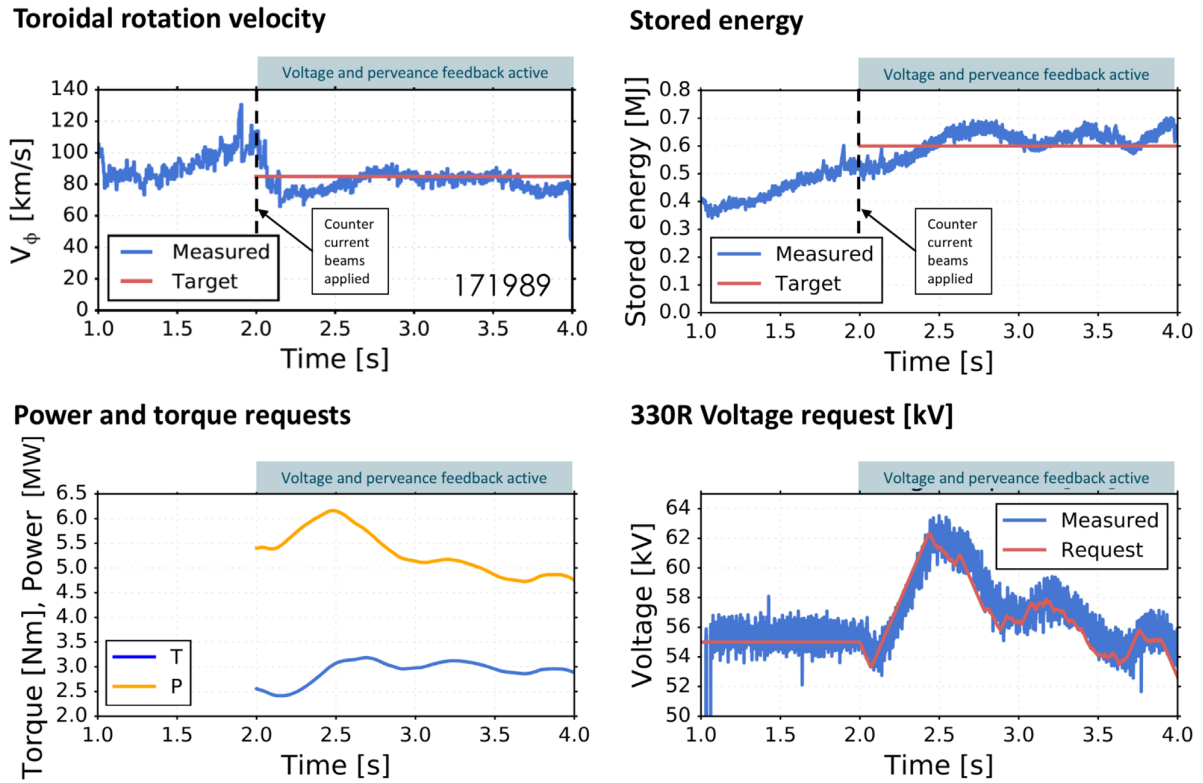


Figure 2. Results from shot 171989 in which voltage changes alone were used to feedback control toroidal rotation (upper left) and stored energy (upper right) starting at 2.0 s. The power and torque requirements calculated by the controller (lower left) were fast enough to hit the beam voltage command rate limits (330R is shown in lower right).

3. Experimental results

In this section, we present experimental results showing the performance of the control scheme during its first tests on the DIII-D device. The first case was from the initial test of the algorithm. Although generally successful, the initial

shots revealed a significant lag between achieved beam current changes and commands that hindered performance. The lag was found to have a time constant of roughly 80 ms (for comparison, the energy confinement time for these shots is between 50–100 ms). The control scheme was later modified to account for this lag. The results of two experimental tests

of the updated algorithm are shown, demonstrating improved performance.

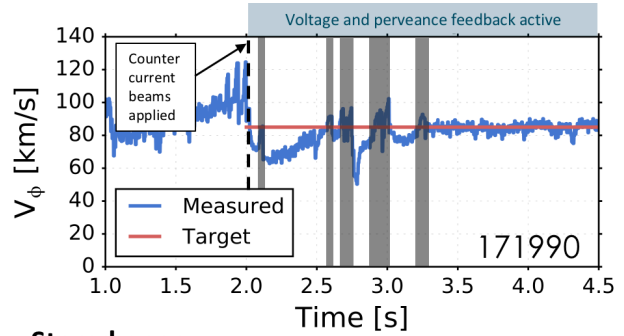
3.1. Stored energy and rotation control with voltage feedback

In shot 171989, the algorithm was configured to simultaneously track targets for stored energy and rotation starting at $t = 2.0$ s. The discharge was ramped up using the modulation based β_N feedback algorithm, using a subset of beams (30R, 150L, 150R, 330L, and 330R). To enable counter-torque during the phase of the discharge testing the new algorithm, the 30R and 150R beams were replaced with 210L and 210R at $t = 2.0$ s, introducing a large disturbance to the beam torque. Beam modulation was also disabled for all beams at this time. The algorithm was configured to change only the voltage of the beams, adjusting the beam current request to maintain optimal perveance throughout the shot. Results of the test are shown in figure 2. At the start of the controlled phase of the shot, both the rotation and stored energy (upper left and right, respectively) differ from their target values and are brought close to the targets by the control algorithm in around 0.5 s. While tracking was generally achieved, oscillations are evident, especially in the stored energy. These result from disturbances (either changes in the confinement or the heating and torque deposition efficiencies of the beams) that were estimated by the observer. The power and torque requests (lower left) were modified to reject the disturbances, however, the changes were fast enough to cause saturation due to the rate limits on the voltage changes. A lag between requested and achieved voltage is also evident. The power and torque changes therefore did not accurately reject the disturbances, indicating that, due to slow response time, voltage changes alone may not be suitable for most feedback applications.

3.2. Stored energy and rotation control with voltage and perveance feedback

In shot 171990, the algorithm was configured to simultaneously track targets for stored energy and rotation starting at $t = 2.0$ s using both beam perveance and voltage changes. Again, beam modulations were disabled during the phase of the discharge in which the algorithm was tested. Results of the test are shown in figure 3. At the start of the controlled phase of the shot, both the rotation and stored energy (upper and middle panels) differ from their target values and are brought close to the targets by the control algorithm in around 0.5 s. Tracking of the targets is also evident after $t = 3.3$ s. During this test, significant disturbances occurred that caused large rapid deviations in the rotation and stored energy (shaded grey regions). These were found to be correlated with occasional sudden cessation of the normally high frequency ELM cycle. ELMs cause frequent short bursts of D_α that appear as vertical lines in the bottom panel of figure 3. The periods of low ELM frequency are indicated with shaded grey boxes in these plots and correspond to the shaded grey regions in the upper panels. During these periods, the confinement evidently increased,

Toroidal rotation velocity



Stored energy

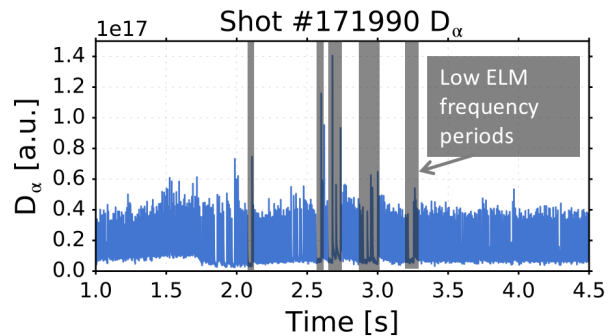
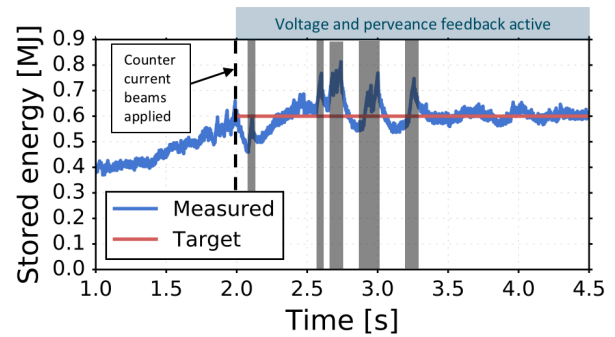


Figure 3. Results from shot 171990 in which both voltage and perveance changes were used to feedback control toroidal rotation (upper) and stored energy (middle) starting at 2.0 s. D_α intensity (lower) shows the presence of ELMs, which cause short, typically frequent, bursts of D_α . Periods of low ELM cycle frequency are evident in the shaded grey regions. The corresponding regions are also shaded grey in the other plots.

resulting in a stored energy rise. The ELM-free phases were each interrupted by large ELMs that suddenly expelled a large fraction of stored energy. While these sudden disturbances occur too quickly for slow voltage changes to compensate, it was expected that fast perveance adjustments could help mitigate their effect on the plasma to some extent. However, analysis of the results showed that, although fast changes in power and torque were requested by the algorithm, the achieved response was slower than anticipated. This was found to be a result of a lag between the requested and achieved beam current that is evident in the left panel of figure 4. The lag was found to have a time constant of roughly 80 ms. An approach

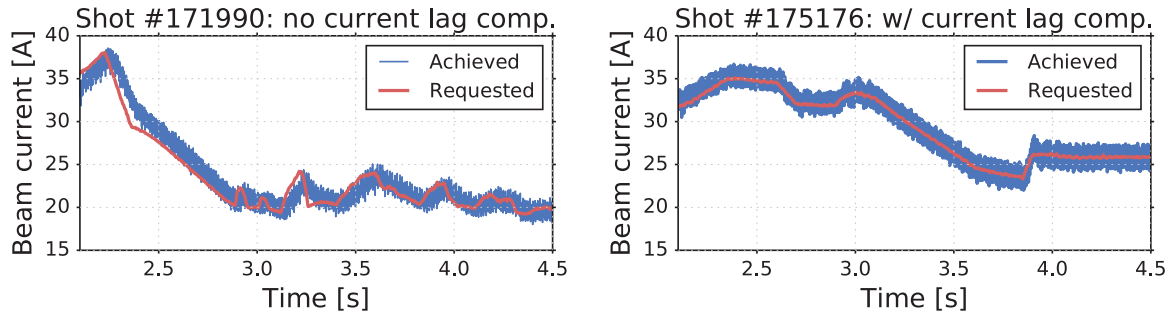


Figure 4. Comparison of beam current request tracking with and without additional feedback.

to compensating for this effect is described and tested in the following section.

3.3. Compensation of lag in beam current changes

To compensate for the lag in beam current changes, a modification to the algorithm was implemented. The modification makes use of the real-time measurements of beam current and adds a proportional feedback term to adjust the beam current commands sent to the beams. This speeds up tracking of the beam current requests that are generated by the constrained optimization algorithm described in section 2. The improvement in beam current tracking is evident in figure 4, which compares tracking during a shot before the modification to tracking after compensation was added. The modification enables faster perveance changes to work as intended in the control design, i.e. to compensate for the very slow response of the voltage actuators. This is demonstrated experimentally in figure 5. The left panel compares achieved accelerator voltage (blue) to the optimal target calculated by the control algorithm (green). The slow response time is evident, even with feedback compensation applied to the voltage commands (red) designed to increase the response time. Despite this, the right panel shows that ramps in torque target were accurately followed as a result of fast changes in beam perveance (the ramps in achieved and requested beam current can be seen in the right panel of figure 4). The accelerator voltage and beam current changes measured by the local beam control system have been confirmed by the Doppler shifted beam emission as measured by the main ion CER system on DIII-D [22].

3.4. Modulation free control at near-zero torque

A final commissioning test was performed in a scenario with beams chosen to produce near-zero torque. Tests of several capabilities were combined into one shot due to experimental time constraints. The shot was configured to use the original modulation based beam control approach for the first 3 s, and the new approach for the remainder of the shot. The control algorithms were configured to control two target quantities at a time, and the specific combination of targets was changed

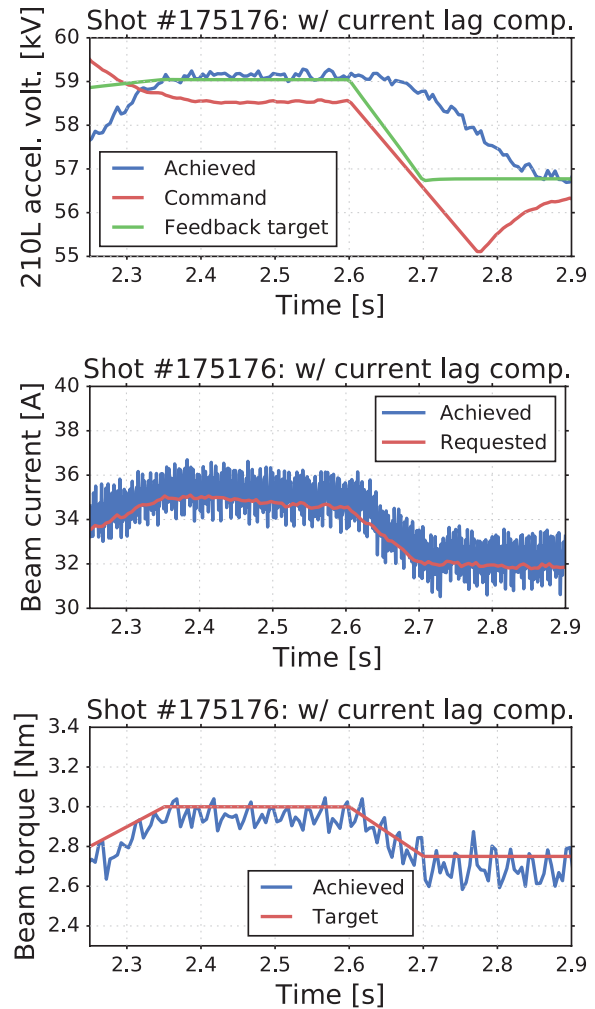


Figure 5. Results of shot 175176 in which beam current lag compensation was enabled. Comparison of achieved 210L accelerator voltage with the optimized target and the command sent to the beams (upper). Comparison of achieved 210L beam current and request (middle). Comparison of achieved and target torque showing that fast tracking of the requested current changes enabled fast torque response despite the slow voltage response (bottom).

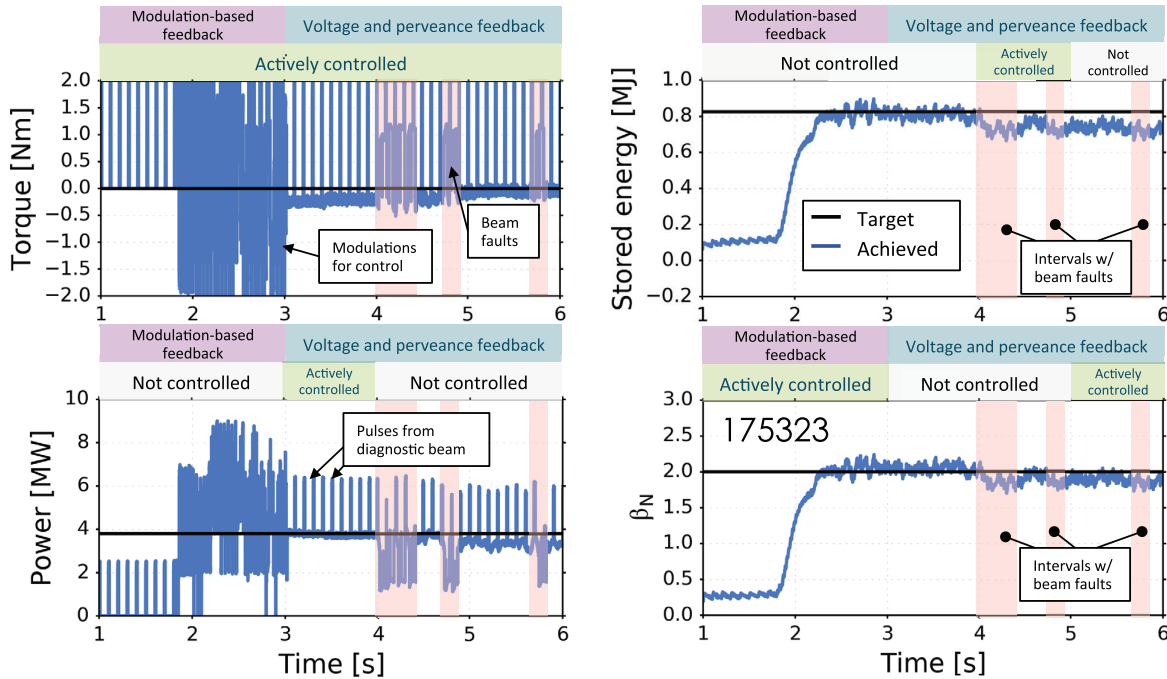


Figure 6. Torque (upper left), power (lower left), stored energy (upper right), and β_N (lower right) from shot 175323. The original modulation-based control scheme was active from $t = 1\text{--}3$ s, while the voltage and perveance feedback scheme was used in the rest of the shot (indicated by top colored bar). The two quantities being actively controlled varied throughout the shot. The interval in which each quantity is actively controlled is indicated by a green bar at the above the figure. Target values are black while achieved values are blue. Controlled modulations, diagnostic beam pulses, and beam faults are also indicated.

at 1 s intervals starting at $t = 3.0$ s. Results from this shot, 175323, are shown in figure 6. The active control scheme and the actively controlled target quantities are indicated by the colored bars at the top of each panel. From $t = 2.0\text{--}3.0$ s, the zero torque condition was achieved using the original beam modulation approach. Although the average torque is near 0 Nm, the modulating beams result in ± 4 Nm swings in applied torque. From $t = 3.0\text{--}4.0$ s, the new algorithm was activated and configured to control power and torque using voltage and perveance changes, with no feedback beam modulations. Accurate tracking of the requests, without large modulations is evident during this period of the discharge. The only modulations are a result of beam blips of 30L used to obtain MSE measurements. From $t = 4.0\text{--}5.0$ s, the algorithm was configured to control torque and stored energy. During this period, some of the beams began to block, resulting in additional modulations and imperfect tracking. However, good tracking of torque and stored energy is evident between the blocks ($t = 4.5\text{--}4.75$ s). Finally, from $t = 5.0\text{--}6.0$ s, the algorithm was configured to track torque and β_N . Tracking of both quantities is evident, with small deviations as a result of beam blocks around $t = 5.75$ s. The beam reliability issues may be a result of changing the beam perveance too far from the optimal value. While limits on the change are incorporated into the control design, the specific values of these limits required to ensure reliable beam operation will have to be refined empirically. The results demonstrate that tracking performance similar to the original modulation-based approach

can be achieved without modulations by using the new actuation capabilities. Due to the smoothing effect of the energy confinement time, the presence of noise in the reconstructed energy and β_N , and the required beam blips for diagnostics, there is not a significant reduction in the variation of stored energy when beam modulations are removed (some slight reduction is apparent in the stored energy and β_N variations at $t = 3$ s when the new approach is activated). However, enabling control without modulations has the benefit of making physics analysis more straightforward (since the applied power and torque are smooth in time) and reduces fatigue on accelerator components and high voltage power supplies.

4. Discussion of results

The results of the experiments demonstrate feedback control of the power, torque, stored energy, and rotation on DIII-D without beam modulations. This is the first feedback algorithm to make use of the expanded controllability of DIII-D enabled by real-time variable beam voltage and perveance. Building upon the previous modulation-based control algorithm, this algorithm includes innovations to address the complexity of the large number of actuators and the constraints that must be respected to ensure beam reliability. The use of real-time constrained optimization enables the control algorithm to minimize the target tracking error within the reliable operating space of the beams. Initial experimental tests of the algorithm demonstrated the capabilities.

The speed of response using voltage changes alone is limited, making it challenging to control even fairly low frequency disturbances without inducing oscillations. Although perveance changes can be made much more quickly, moving the perveance too far from optimal can cause beam reliability issues. The presented control scheme overcomes these challenges by combining the two approaches, enabling perveance changes to compensate for the slow voltage response time, while voltage changes provide control at low frequencies. Since the voltage and perveance changes are magnitude limited, the controllable range for a given set of active beams is constrained. Though not demonstrated here, the proposed control algorithm can be configured to allow the use of beam modulations in combination with voltage and perveance changes to expand the controllable range. Through proper choice of relative weighting on the actuators, the algorithm can be configured to only use beam modulations if the tracking error is too large to reject with voltage and perveance changes alone. The proposed scheme provides a computationally inexpensive but sub-optimal solution to this problem; for experiments requiring minimal modulation of beams through a large range of power and torque changes, selection of the active set of beams and their voltages and perveances at any given time requires solution of a constrained mixed integer optimization problem. A model predictive control approach [23] may be required to optimally solve this problem in real-time, at the cost of significantly more computational time. The model predictive control approach will be assessed in future work.

While there are challenges to incorporating voltage and perveance feedback in algorithms, the approach demonstrated here motivates the development of more sophisticated applications of the new capabilities. The controlled outputs will be extended in the future to include ECE measurements of mode amplitude, enabling smooth, precise feedback control over toroidal Alfvén eigenmode activity. Control of mode activity could be an important tool, especially when integrated with profile control strategies, for improving reproducibility and performance of steady-state scenarios on DIII-D [24]. Integrated active fast-ion-phase-space control and scenario control could be an important capability for achieving and maintaining advanced reactor scenarios, and the ability to perform control through smooth variations of beam power and energy (as opposed to pulse width modulation) could increase device reliability by reducing fatigue on beam system components.

Acknowledgments

This work was supported by the US Department of Energy Grant under contract number DE-AC02-09CH11466. This material is based upon work supported by the US Department of Energy, Office of Science, Office of Fusion Energy Sciences, using the DIII-D National Fusion Facility, a DOE Office of Science user facility, under Awards DE-FC02-04ER54698. DIII-D data shown in this paper can be obtained in digital format by following the links at https://fusion.gat.com/global/D3D_DMP

This report was prepared as an account of work sponsored by an agency of the United States Government. Neither the United States Government nor any agency thereof, nor any of their employees, makes any warranty, express or implied, or assumes any legal liability or responsibility for the accuracy, completeness, or usefulness of any information, apparatus, product, or process disclosed, or represents that its use would not infringe privately owned rights. Reference herein to any specific commercial product, process, or service by trade name, trademark, manufacturer, or otherwise does not necessarily constitute or imply its endorsement, recommendation, or favoring by the United States Government or any agency thereof. The views and opinions of authors expressed herein do not necessarily state or reflect those of the United States Government or any agency thereof.

Appendix A. Model for control design

A.1. Power and torque dependence on voltage and perveance

For the j th source, the power from the ion source is determined by the acceleration voltage, V_j , and the source perveance, $\Pi_j = I_j/V_j^{3/2}$ (where I_j is the source current), while the actual power that reaches the plasma is decreased by a number of loss mechanisms. The losses are represented as efficiency coefficients in the calculation of power. Those considered in this work are: transmission (loss of beam that is intercepted by grids), neutralization efficiency, reionization loss, drift-duct loss, and beam overlap loss. The transmission and neutralization efficiency coefficients, $\epsilon_{t,j}$, and $\epsilon_{n,j}$ depend on the voltage, perveance, and gas flow rates, and are approximated as:

$$\epsilon_{t,j} = a_{t,j}\Pi_j^3 + b_{t,j}\Pi_j^2 + c_{t,j}\Pi_j + d_{t,j}, \quad (\text{A.1})$$

$$\epsilon_{n,j} = L_{NEq,i,j}(a_{n,j}V_j + b_{n,j}). \quad (\text{A.2})$$

The gas flow rate dependence is calculated as

$$L_{NEq,i,j} = 1 - e^{-0.1034(q_{nz} + q_{src} - q_{beam})}, \quad (\text{A.3})$$

where q_{nz} and q_{src} are the neutralizer and source gas flow rates in $T - l/s$, respectively, and $q_{beam} = 0.8435 + 0.0336\Pi_j^{3/2}$. The power reaching the plasma for the j th source is given by

$$P_j = f_d L_R L_{dd} L_{overlap} \epsilon_{t,j} \epsilon_{n,j} I_j V_j, \quad (\text{A.4})$$

where f_d is the duty cycle of the beam and the current is related to the beam perveance by

$$I_j = \Pi_j V_j^{3/2}. \quad (\text{A.5})$$

The torque from the j th source is given by

$$T_j = R_{tan} P_j \sum_{i=1}^3 f_{p,i,j} \sqrt{\frac{2m_p \mu i}{eV_j}}, \quad (\text{A.6})$$

where R_{tan} is the tangency radius of the beam, m_p is the mass of a proton, e is the electron charge, and μ is taken as two for deuterium beams. An example of the power and torque

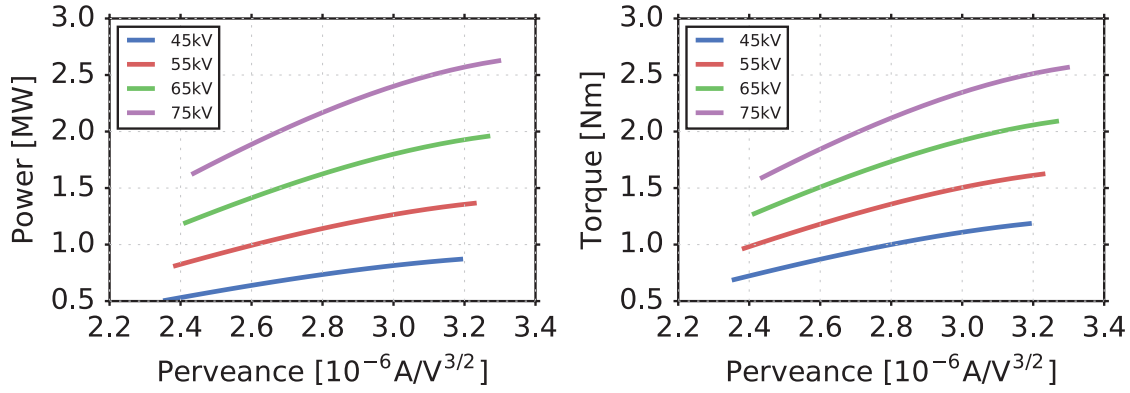


Figure A1. Dependence of (left) power and (right) torque on perveance and voltage for beam 330L.

dependence on voltage and perveance for beam 330L is shown in figure A1.

The fraction of power for each energy fraction (full, half, and a third) of the beam ion population are calculated as weighted sums of the currents fractions,

$$f_{p,i} = \frac{f_{c,i}/i}{\sum_{j=1}^3 f_{c,j}/j}. \quad (\text{A.7})$$

The current fractions are calculated from fitted polynomial functions of the injection voltage:

$$f_{c,1} = a_{fc,1} + b_{fc,1}V_j + c_{fc,1}V_j^2 \quad (\text{A.8})$$

$$f_{c,2} = a_{fc,2} + b_{fc,2}V_j + c_{fc,2}V_j^2 \quad (\text{A.9})$$

$$f_{c,3} = 1 - f_{c,1} - f_{c,2}. \quad (\text{A.10})$$

A.2. Beam dynamics

The local control circuitry for each beam effectively low-pass filters the voltage commands sent from the PCS, resulting in the dynamic response

$$\dot{V}_j = \frac{-V_j + V_{\text{com},j}}{\tau_{V,j}}. \quad (\text{A.11})$$

The source density, and hence source current, is regulated by a local beam control system. The average voltage generated by the ion collection currents from a set Langmuir probes at the entrance to the accelerator and their associated burden resistors is regulated to a target value, V_{probe} by adjusting the arc voltage. Real-time control of the source current from PCS is achieved by sending an offset voltage to the nominal value of V_{probe} set by the beam operators before the shot. The offset voltage, ΔV_{probe} results in an approximately linear change in source current, and the local control system achieves a dynamic response that can approximately be represented by a first-order low-pass filter, i.e.

$$\Delta \dot{I}_j = \frac{-\Delta I_j + k_{\text{probe},j} \Delta V_{\text{probe},j}}{\tau_{I,j}}, \quad (\text{A.12})$$

where $k_{\text{probe},j}$ is a source dependent coefficient.

A.3. Stored energy and rotation

The stored energy, E , and rotation frequency, ω , are modeled with a simplified relationship similar to the one used in [12]:

$$\dot{E} = P - \frac{E}{\tau_E}, \quad (\text{A.13})$$

$$\dot{v}_{\text{rot}} = \frac{T}{n_i m_i R_0} - \frac{v_{\text{rot}}}{\tau_m}, \quad (\text{A.14})$$

where $P = \sum_{j=1}^{N_b} P_j$, $T = \sum_{j=1}^{N_b} T_j$, $N_b = 8$ is the number of beams, τ_E and τ_m are the energy and momentum confinement times, respectively. The confinement times were assumed to be $\tau_E = \tau_m = 0.1$ during experimental testing, based on the confinement achieved in similar reference discharges. n_i and m_i are the ion density, approximated as being constant, and mass. R_0 is the plasma major radius.

Appendix B. Control algorithm design details

B.1. Observer and parameter estimation

To estimate the stored energy, rotation, and model parameters in real-time from the noisy measurements, an observer is designed of the form

$$\dot{\hat{E}} = P - \frac{\hat{E}}{\tau_E} + \hat{d}_E - L_E \tilde{E}, \quad (\text{B.1})$$

$$\dot{\hat{v}}_{\text{rot}} = \frac{T}{n_i m_i R_0} - \frac{\hat{v}_{\text{rot}}}{\tau_m} + \hat{d}_m - L_m \tilde{v}_{\text{rot}}, \quad (\text{B.2})$$

where \hat{E} , \hat{v}_{rot} are the estimated stored energy, and rotation, and the terms \hat{d}_E , and \hat{d}_m are estimates of additive disturbances. The estimation errors are denoted as $\tilde{E} = \hat{E} - E$ and $\tilde{v}_{\text{rot}} = \hat{v}_{\text{rot}} - v_{\text{rot}}$. The output injection gains L_E and L_m are positive scalar design parameters for improving the response time of the estimation error. The dynamics of the estimation error are given by

$$\dot{\tilde{E}} = -\frac{\tilde{E}}{\tau_E} + \tilde{d}_E - L_E \tilde{E}, \quad (\text{B.3})$$

$$\dot{\hat{v}}_{\text{rot}} = -\frac{\tilde{v}_{\text{rot}}}{\tau_m} + \tilde{d}_m - L_m \tilde{v}_{\text{rot}}. \quad (\text{B.4})$$

The estimated disturbances are updated according to

$$\dot{\hat{d}}_E = -k_E \tilde{E}, \quad (\text{B.5})$$

$$\dot{\hat{d}}_m = -k_m \tilde{v}_{\text{rot}}, \quad (\text{B.6})$$

where k_E and k_m are positive semi-definite design parameters. The disturbance estimates are projected to satisfy an assumed set of minimum and maximum values, i.e. $d_{E\text{min}} \leq \hat{d}_E \leq d_{E\text{max}}$ and $d_{m\text{min}} \leq \hat{d}_m \leq d_{m\text{max}}$. Assuming constant disturbances, the estimation error systems converge to zero at steady-state, and the design parameters L_E , L_m , k_E , and k_m enable tuning the response of the estimators.

B.2. Actuator grouping

To enable a reduction of the computational complexity of the optimization problem and ensure the $<20 \mu\text{s}$ total execution time of each cycle of the algorithm is achievable, each of the beam injectors is assigned to one of $N_g \leq N_b$ groups. Following the approach used in the previous duty-cycle-based approach, the initial implementation of the algorithm uses two groups of beams. To maximize the controllable range of power and torque with the two groups, it is best for the power and torque produced by the two groups to be as orthogonal as possible. Therefore, the first group is typically assigned all of the co-injection beams and the second group is assigned all of the counter-injection beams.

The voltages, perveances, and duty cycles of the sources within the i th group are coupled together through a new set of normalized actuators α_i , β_i , γ_i . These variables are used to interpolate between the minimum and maximum parameters of the sources within the group. Taking the j th source in the i th group as an example:

$$V_{i,j} = (V_{i,j,\text{max}} - V_{i,j,\text{min}})\alpha_i + V_{i,j,\text{min}}, \quad (\text{B.7})$$

$$P_{i,j} = (P_{i,j,\text{max}} - P_{i,j,\text{min}})\beta_i + P_{i,j,\text{min}}, \quad (\text{B.8})$$

$$\theta_{i,j} = (\theta_{i,j,\text{max}} - \theta_{i,j,\text{min}})\gamma_i + \theta_{i,j,\text{min}}. \quad (\text{B.9})$$

The vector of normalized actuators for each group is denoted as $u_i = [\alpha_i, \beta_i, \gamma_i]^T$. The vectors for each group are concatenated to form the actuator vector $u \in \mathbb{R}^{3 \times N_g}$. In the subsequent sections, optimization will be done over the reduced set of $3N_g = 6$ actuator variables in the vector u .

Generalizing relations (B.7)–(B.9), the complete vector of actuator values for each individual source, $v \in \mathbb{R}^{3N_b \times 1}$, can be written as

$$v = DMu + v_{\text{min}} \quad (\text{B.10})$$

where $v_{\text{min}} \in \mathbb{R}^{3N_b \times 1}$ is an array of the minimum allowed value for each of the actuators, the matrix $M \in \mathbb{R}^{3N_b \times 3N_g}$

maps normalized group actuators to individual beam actuators, and the matrix $D \in \mathbb{R}^{3N_b \times 3N_b}$ is a diagonal matrix with its diagonal elements given by the range of each individual beam actuator.

B.3. Feedforward control

The estimated model, which converges to zero estimation error at steady-state under the effect of constant disturbances, is used in real-time to determine the feedforward actuator commands that will reject the disturbance while optimally tracking operator specified target stored energy and rotation values at steady-state, subject to the actuator constraints. Only steady-state constraints are considered in this optimization problem (i.e. rate limits are ignored). The steady-state output of the estimated model is given by

$$\hat{E}_{\text{ss}} = \tau_E (P_{\text{ss}} + \hat{d}_E), \quad (\text{B.11})$$

$$\hat{v}_{\text{rot,ss}} = \tau_m \left(\frac{T_{\text{ss}}}{n_i m_i R_0} + \hat{d}_m \right). \quad (\text{B.12})$$

The vector of optimized, normalized actuator requests to be calculated in this step is denoted as u_{ss} . The optimized feedforward individual beam actuator requests v_{ss} are related to this vector as

$$v_{\text{ss}} = D_{\text{ss}} M u_{\text{ss}} + v_{\text{min,ss}} \quad (\text{B.13})$$

where $v_{\text{min,ss}}$ is the vector of minimum values of the individual source actuator values allowed at steady-state, and the diagonal elements of D_{ss} are the range of individual source actuator values allowed at steady-state. These values are configured by the operator for each shot based on beam limits and experiment requirements. The perveance minimum and maximum are defined by the operator in terms of fractions (typically 0.9 and 1.1, respectively) of the voltage-dependent optimal perveance for each source. At each cycle of the control algorithm, the optimal perveance is calculated for the measured source voltage using a look-up table, and the absolute limits are calculated using the operator specified fractions. Since the power and torque depend nonlinearly on the controlled variables, at each sample time, the expressions for power and torque are linearized with respect to the normalized actuators around the values from the previous cycle, e.g.

$$P_{\text{ss}} \approx P_{\text{ss},0} + F_{\text{ss},P} \Delta u_{\text{ss}}, \quad (\text{B.14})$$

$$T_{\text{ss}} \approx T_{\text{ss},0} + F_{\text{ss},T} \Delta u_{\text{ss}}, \quad (\text{B.15})$$

where the vector of optimized, normalized values from the values u_{ss} from the last cycle of the algorithm is denoted $u_{\text{ss},0}$, and the associated power and torque are denoted as $P_{\text{ss},0}$ and $T_{\text{ss},0}$, respectively. Δu_{ss} represents the vector of deviations of u_{ss} from the values on the previous cycle, while the matrices $F_{\text{ss},P}$ and $F_{\text{ss},T}$ are given by

$$F_{ss,P} = \begin{bmatrix} \sum_{j=1}^{N_b} \frac{\partial P_j}{\partial \alpha_{co}} \Big|_{u_{ss,0}} \\ \sum_{j=1}^{N_b} \frac{\partial P_j}{\partial \beta_{co}} \Big|_{u_{ss,0}} \\ \sum_{j=1}^{N_b} \frac{\partial P_j}{\partial \gamma_{co}} \Big|_{u_{ss,0}} \\ \sum_{j=1}^{N_b} \frac{\partial P_j}{\partial \alpha_{ctr}} \Big|_{u_{ss,0}} \\ \sum_{j=1}^{N_b} \frac{\partial P_j}{\partial \beta_{ctr}} \Big|_{u_{ss,0}} \\ \sum_{j=1}^{N_b} \frac{\partial P_j}{\partial \gamma_{ctr}} \Big|_{u_{ss,0}} \end{bmatrix}^T, F_{ss,T} = \begin{bmatrix} \sum_{j=1}^{N_b} \frac{\partial T_j}{\partial \alpha_{co}} \Big|_{u_{ss,0}} \\ \sum_{j=1}^{N_b} \frac{\partial T_j}{\partial \beta_{co}} \Big|_{u_{ss,0}} \\ \sum_{j=1}^{N_b} \frac{\partial T_j}{\partial \gamma_{co}} \Big|_{u_{ss,0}} \\ \sum_{j=1}^{N_b} \frac{\partial T_j}{\partial \alpha_{ctr}} \Big|_{u_{ss,0}} \\ \sum_{j=1}^{N_b} \frac{\partial T_j}{\partial \beta_{ctr}} \Big|_{u_{ss,0}} \\ \sum_{j=1}^{N_b} \frac{\partial T_j}{\partial \gamma_{ctr}} \Big|_{u_{ss,0}} \end{bmatrix}^T. \quad (\text{B.16})$$

Expressions (B.14) and (B.15) can be used to write the estimated steady-state tracking error, $e_{ss} = [\hat{E}_{ss} - E_t, \hat{v}_{rot,ss} - v_{rot,t}]^T$ as:

$$e_{ss} = G_{ss} \Delta u_{ss} + H_{ss}, \quad (\text{B.17})$$

where

$$G_{ss} = \begin{bmatrix} \tau_E F_{ss,P} \\ \tau_m F_{ss,T} \end{bmatrix}, \quad (\text{B.18})$$

$$H_{ss} = \begin{bmatrix} \tau_E (P_{ss,0} + \hat{d}_E) - E_t \\ \tau_m (T_{ss,0} + \hat{d}_m) - v_{rot,t} \end{bmatrix}. \quad (\text{B.19})$$

To find actuator commands that minimize the steady-state error (B.17) while weighting the deviation of the actuators from their pre-programmed reference values (denoted $\tilde{v}_{ss} = v_{ss} - v_{ref}$), the minimization of the cost function

$$J_{ss,0} = \frac{1}{2} e_{ss}^T Q_{ss} e_{ss} + \frac{1}{2} \tilde{v}_{ss}^T R_{ss} \tilde{v}_{ss} \quad (\text{B.20})$$

is considered. In (B.20), $Q_{ss} \in \mathbb{R}^{2 \times 2}$ is a positive definite matrix weighting the steady-state tracking errors and $R_{ss} \in \mathbb{R}^{6 \times 6}$ is a positive definite matrix weighting the deviation of the actuators. This is equivalent to the minimization of

$$J_{ss} = \frac{1}{2} \Delta u_{ss}^T \Gamma_{ss} \Delta u_{ss} + \Delta u_{ss}^T \Phi_{ss}, \quad (\text{B.21})$$

where

$$\Gamma_{ss} = G_{ss}^T Q_{ss} G_{ss} + M^T D_{ss}^T R_{ss} D_{ss} M, \quad (\text{B.22})$$

$$\Phi_{ss} = G_{ss}^T Q_{ss} H_{ss} + M^T D_{ss}^T R_{ss} (D_{ss} M u_{ss,0} - v_{ref}). \quad (\text{B.23})$$

At each sample time, an iteration of a box constrained quadratic program solver is used to produce a sub-optimal solution Δu_{ss}^* subject to the constraints:

$$\Delta u_{ss,\min} = -u_{ss,0}, \quad (\text{B.24})$$

$$\Delta u_{ss,\max} = 1 - u_{ss,0}. \quad (\text{B.25})$$

Based on the definition of the normalized actuator values u_{ss} , the constraints (B.24) and (B.25) are equivalent to constraining the manipulated variables to within their allowable magnitude ranges. Though only one iteration of the optimizer is performed per cycle of the algorithm, for fixed or slowly

varying weights, targets, and disturbance estimates, the algorithm converges to the optimal solution over a small number of cycles. The steady-state power and torque values associated with $u_{ss}^* = u_{ss,0} + \Delta u_{ss}^*$ are denoted as P_{ss}^* and T_{ss}^* and the corresponding steady-state outputs (referred to later as the steady-state achievable targets) associated with these values are denoted E_{ss}^* and $v_{rot,ss}^*$.

B.4. Feedback control

While the power and torque calculated in the previous section would cause the system (A.13) and (A.14) to evolve to a steady-state that minimizes the cost function (B.20), the time response may be slower than desired, especially when the voltage rate limits and lag are considered. In this section, the power and torque requests are augmented with a feedback term and the perveance and duty cycle requests are optimized, subject to magnitude limits, to best track these requests. Due to its slow response time from slew rate limits and lag, the beam voltage is not suitable for fast transient response and is considered fixed at its estimated present value for the purposes of this optimization problem. The power and torque feedback terms are calculated as

$$P_{fb} = -k_{E,fb} (\hat{E} - E_{ss}^*), \quad (\text{B.26})$$

$$T_{fb} = -k_{m,fb} (\hat{v}_{rot} - v_{rot,ss}^*), \quad (\text{B.27})$$

and are added to the requests resulting from the feedforward calculations to produce the total power and torque requests

$$P_{req} = P_{ss}^* + P_{fb}, \quad (\text{B.28})$$

$$T_{req} = T_{ss}^* + T_{fb}. \quad (\text{B.29})$$

The vector of optimized, normalized actuator requests to be calculated in this step is denoted as u . The optimized individual beam actuator requests v are related to this vector as

$$v = DMu + v_{\min} \quad (\text{B.30})$$

where v_{\min} is the vector of minimum values of the individual source actuator values allowed at steady-state, and the diagonal elements of D are the range of individual source actuator values allowed at steady-state. The limits for perveance and duty cycle used in this step can differ from those used in the previous step, and are configured by the operator for each shot based on beam limits and experiment requirements. The perveance minimum and maximum are again defined by the operator in terms of fractions of the voltage-dependent optimal perveance for each source and calculated based on the measured source voltage. As previously mentioned, in this step, the voltage requests are constrained to match the measured values, such that the remaining free actuators will be optimized to achieve the required power and torque as closely as possible, compensating for the slow response of the beam voltage. As in the previous section, since the power and torque depend nonlinearly on the controlled variables, at each sample time, the expressions for power and torque are linearized with

respect to the normalized actuators around the values from this calculation on the previous cycle, e.g.

$$P \approx P_0 + F_P \Delta u, \quad (\text{B.31})$$

$$T \approx T_0 + F_T \Delta u, \quad (\text{B.32})$$

where Δu represents the vector of deviations of u from the values on the previous cycle, while the matrices F_P and F_T are given by

$$F_P = \begin{bmatrix} \sum_{j=1}^{N_b} \frac{\partial P_j}{\partial \alpha_{co}} \Big|_{u_0} \\ \sum_{j=1}^{N_b} \frac{\partial P_j}{\partial \beta_{co}} \Big|_{u_0} \\ \sum_{j=1}^{N_b} \frac{\partial P_j}{\partial \gamma_{co}} \Big|_{u_0} \\ \sum_{j=1}^{N_b} \frac{\partial P_j}{\partial \alpha_{cntr}} \Big|_{u_0} \\ \sum_{j=1}^{N_b} \frac{\partial P_j}{\partial \beta_{cntr}} \Big|_{u_0} \\ \sum_{j=1}^{N_b} \frac{\partial P_j}{\partial \gamma_{cntr}} \Big|_{u_0} \end{bmatrix}^T, \quad F_T = \begin{bmatrix} \sum_{j=1}^{N_b} \frac{\partial T_j}{\partial \alpha_{co}} \Big|_{u_0} \\ \sum_{j=1}^{N_b} \frac{\partial T_j}{\partial \beta_{co}} \Big|_{u_0} \\ \sum_{j=1}^{N_b} \frac{\partial T_j}{\partial \gamma_{co}} \Big|_{u_0} \\ \sum_{j=1}^{N_b} \frac{\partial T_j}{\partial \alpha_{cntr}} \Big|_{u_0} \\ \sum_{j=1}^{N_b} \frac{\partial T_j}{\partial \beta_{cntr}} \Big|_{u_0} \\ \sum_{j=1}^{N_b} \frac{\partial T_j}{\partial \gamma_{cntr}} \Big|_{u_0} \end{bmatrix}^T. \quad (\text{B.33})$$

The error between the power and torque and the requests calculated in (B.28) and (B.29) is denoted as

$$e = [P - P_{\text{req}}, T - T_{\text{req}}]^T, \quad (\text{B.34})$$

which can be expressed as:

$$e = G \Delta u + H, \quad (\text{B.35})$$

where

$$G = \begin{bmatrix} F_P \\ F_T \end{bmatrix}, \quad (\text{B.36})$$

$$H = \begin{bmatrix} P_0 - P_{\text{req}} \\ T_0 - T_{\text{req}} \end{bmatrix}. \quad (\text{B.37})$$

To find the actuator commands that minimize the error (B.34) while weighting the deviation of the actuators from their pre-programmed reference values (denoted $\tilde{v} = v - v_{\text{ref}}$), the minimization of the cost function

$$J_0 = \frac{1}{2} e^T Q e + \tilde{v}^T R \tilde{v}, \quad (\text{B.38})$$

is considered. Minimization of this function is equivalent to minimization of

$$J = \frac{1}{2} \Delta u^T \Gamma \Delta u + \Delta u^T \Phi, \quad (\text{B.39})$$

where

$$\Gamma = G^T Q G + M^T D^T R D M, \quad (\text{B.40})$$

$$\Phi = G^T Q H + M^T D^T R (D u + v_{\text{min}} - v_{\text{ref}}). \quad (\text{B.41})$$

At each sample time, an iteration of a box constrained quadratic program solver is used to produce a sub-optimal solution Δu^* subject to the constraints:

$$\Delta u_{\text{min}} = -u_0, \quad (\text{B.42})$$

$$\Delta u_{\text{max}} = 1 - u_0. \quad (\text{B.43})$$

Based on the definition of the normalized actuator values u , the constraints (B.42) and (B.43) are equivalent to constraining the manipulated variables to within their allowable magnitude ranges. Though only one iteration of the optimizer is performed per cycle of the algorithm, for fixed or slowly varying weights, targets, and disturbance estimates, the algorithm converges to the optimal solution over a small number of cycles. The power and torque values associated with $u^* = u_0 + \Delta u^*$ are denoted as P^* and T^* .

The optimal solution u^* is then converted to voltage, perveance, and duty cycle commands.

B.5. Voltage and beam current commands

In order to improve the response time of the beam voltage, the voltage commands calculated in equation (B.13) are augmented with a proportional feedback term, i.e.

$$V_{\text{com},i,j} = V_{\text{ss},i,j} - k_{V,i,j} (\hat{V}_{i,j} - V_{\text{ss},i,j}). \quad (\text{B.44})$$

To avoid tripping the bending magnet current interlocks, these commands are rate limited. Since the local control systems for the beams expects the commands to be in the form of an offset from the nominal pre-shot voltage setting, the nominal value is subtracted from the rate limited command prior to being communicated.

In order to improve the response time of the source current and improve tracking of the perveance requested in equation (B.30), a perveance control algorithm was implemented. The target source current for a requested perveance is calculated based on an estimate of the present beam voltage as

$$I_{\text{req},j} = \Pi_{\text{req},j} \hat{V}_j^{3/2}, \quad (\text{B.45})$$

and the probe voltage offset command to be sent to the local control system is calculated as

$$\Delta V_{\text{probe},j} = \frac{I_{\text{req},j} - \Pi_{\text{opt},j} (V_{0,j}) V_{0,j}^{3/2}}{k_{\text{probe},j}} - \frac{k_{\Pi} \tau_i}{k_{\text{probe},j}} (\hat{I}_j - I_{\text{req},j}). \quad (\text{B.46})$$

ORCID iDs

M.D. Boyer  <https://orcid.org/0000-0002-6845-9155>
 K.G. Erickson  <https://orcid.org/0000-0003-1216-8719>
 B.A. Grierson  <https://orcid.org/0000-0001-5918-6506>
 D.C. Pace  <https://orcid.org/0000-0002-7039-0011>
 J.T. Scoville  <https://orcid.org/0000-0002-2884-7022>
 J. Rauch  <https://orcid.org/0000-0003-0171-1720>
 B.J. Crowley  <https://orcid.org/0000-0002-8005-9437>
 J.R. Ferron  <https://orcid.org/0000-0002-2693-5870>
 S.R. Haskey  <https://orcid.org/0000-0002-9978-6597>
 D.A. Humphreys  <https://orcid.org/0000-0002-0879-4074>
 R. Nazikian  <https://orcid.org/0000-0001-6235-6692>
 C. Pawley  <https://orcid.org/0000-0001-8135-2945>

References

- [1] Homfray D.A. et al 2011 *Fusion Eng. Des.* **86** 780–4
- [2] Uhlemann R. and Ongena J. 1999 *Fusion Technol.* **35** 42
- [3] Scoville J.T., Boyer M.D., Crowley B.J., Eidiotis N.W., Pawley C.J. and Rauch J.M. 2018 *Fusion Eng. Des.* accepted (<https://doi.org/10.1016/j.fusengdes.2018.10.015>)
- [4] Crowley B., Rauch J. and Scoville J.T. 2015 *Fusion Eng. Des.* **96–7** 443
- [5] Holcomb C.T. et al 2015 *Phys. Plasmas* **22** 055904
- [6] Heidbrink W.W. et al 2014 *Plasma Phys. Control. Fusion* **56** 095030
- [7] Fredrickson E.D. et al 2017 *Phys. Rev. Lett.* **118** 265001
- [8] Pawley C.J., Crowley B.J., Pace D.C., Rauch J.M., Scoville J.T., Kellman D.H. and Kellman A.G. 2017 *Fusion Eng. Des.* **123** 453
- [9] Rauch J., Pace D.C., Crowley B., Johnson R.D., Kellman D.H., Pawley C.J. and Scoville J.T. 2017 *Fusion Sci. Technol.* **72** 500–4
- [10] Pace D.C. et al 2018 *Phys. Plasmas* **25** 056109
- [11] Pace D.C. et al 2017 *Nucl. Fusion* **57** 014001
- [12] Scoville J.T., Humphreys D.A., Ferron J.R. and Gohil P. 2007 *Fusion Eng. Des.* **82** 1045
- [13] Schuster E. et al 2017 *Nucl. Fusion* **57** 116026
- [14] Boyer M.D., Barton J., Schuster E., Luce T.C., Ferron J.R., Walker M.L., Humphreys D.A., Penaflor B.G. and Johnson R.D. 2013 *Plasma Phys. Control. Fusion* **55** 105007
- [15] Barton J.E., Boyer M.D., Shi W., Schuster E., Luce T.C., Ferron J.R., Walker M.L., Humphreys D.A., Penaflor B.G. and Johnson R.D. 2012 *Nucl. Fusion* **52** 123018
- [16] Ferron J. 2006 *Nucl. Fusion* **46** L13
- [17] Hu W. et al 2018 *Nucl. Fusion* **58** 124001
- [18] Penaflor B.G., Ferron J.R., Hyatt A.W., Walker M.L., Johnson R.D., Piglowski D.A., Kolemen E., Welander A.S. and Lanctot M.J. 2013 Latest advancements in DIII-D plasma control software and hardware *IEEE 25th Symp. on Fusion Engineering (San Francisco, CA, 10–14 June 2013)* (<https://ieeexplore.ieee.org/document/6635496>)
- [19] Ferron J.R., Penaflor B., Walker M.L., Moller J. and Butner D. 1995 *Proc. 16th International Symposium on Fusion Engineering (Champaign, IL, 30 September–5 October 1995)*, vol 2, pp 870–3 (<https://ieeexplore.ieee.org/document/534361>)
- [20] Ferron J., Walker M., Lao L., John H., Humphreys D. and Leuer J. 1998 *Nucl. Fusion* **38** 1055
- [21] Boyer M., Andre R., Gates D., Gerhardt S., Menard J. and Poli F. 2017 *Nucl. Fusion* **57** 066017
- [22] Haskey S.R. et al 2018 *Rev. Sci. Instrum.* **89** 10D110
- [23] Maciejowski J.M. 2002 *Predictive Control: with Constraints* (Harlow, UK: Prentice Hall)
- [24] Holcomb C.T. et al 2014 *Nucl. Fusion* **54** 093009